WOOD RESEARCH
64 (2): 2019
317-324

SUSTAINABLE ACTIVATED CARBON HOLLOW FIBERS FROM LIQUEFIED RUBBER WOOD (*HEVEA BRASILIENSIS*) AND ITS ADSORPTION OF ORGANIC MATTER FROM SOLUTION

Dong-Na Li
Tianjin University of Science and Technology
College of Packaging and Printing Engineering
Tianjin, China

Jia-Ning Li
Chinese Academy of Tropical Agricultural Sciences
Rubber Research Institute, Ministry of Agriculture Key Laboratory of Biology and Genetic Resource Utilization of Rubber Tree, State Key Laboratory Breeding Base of Cultivation and Physiology for Tropical Crops
Danzhou, China

Xiao-Jun Ma
Tianjin University of Science And Technology,College of Packaging and Printing Engineering
Tianjin, China

(Received April 2018)

ABSTRACT

Wooden activated carbon hollow fiber (WACHF) is successfully synthesized from liquefied rubber wood (*Hevea brasiliensis*) using H_2O activation. The structures of WACHF are studied by scanning electron microscope (SEM), X-ray diffraction (XRD) and N_2 adsorption. The effects of activation temperature on methylene blue (MB) and iodine adsorption property were also studied. Results show that both wood hollow fiber (WHF) and WACHF have a smooth surface and hollow fibrous structure with an average hollowness of about 76.43%. With increased activation temperature, the graphite-like microcrystalline structure has been formed. In addition, WACHF has high Brunauer-Emmett-Teller (BET) surface area (1949 $m^2 \cdot g^{-1}$) and total pore volume (1.246 $cm^3 \cdot g^{-1}$), where the contribution for micropores is 47.4% and 46.3% for the mesopores. At 800°C, the MB adsorption and iodine adsorption of WACHF reach the maximal

values of 412.6 $mg \cdot g^{-1}$ and 1123.7 $mg \cdot g^{-1}$, respectively. As a result, WACHF with double surface structures has great BET surface area and excellent adsorption property.

KEYWORDS: Wooden activated carbon hollow fibers, activation temperature, methylene blue adsorption, iodine adsorption.

INTRODUCTION

Activated carbon fibers (ACF) have played a major role in adsorption technology with its high and fast adsorption and desorption property and convenient processing. Thus, ACF materials are extensively used to air filters, air purification, solvent recovery, and carrier materials of photocatalyst (Diez et al. 2014, Liu et al. 2015).

ACF is mainly prepared from fossil resource such as polyacrylonitrile (PAN), phenolic, or pitch fibers (Li et al. 1998, Ryu et al. 1998, Hamada et al. 1988). As the shortage of fossil resources, it is necessary to improve the production of ACF which highly depends on chemical materials. Using renewable biomass-based resources as raw materials are particularly important. In recent years, some scientists have paid attention to the biomass-based ACF. For example, they prepared oil palm fiber (Tan et al. 2007, Qoi et al. 2017), jute or flax-ACF (Rombaldo et al. 2014, Kwiatkowski 2017), coconut shell fibers (Shrestha et al. 2013, Shrestha et al. 2014, Thitame and Shukla 2016), lignin-based ACF (Yu et al. 2016, Lin and Zhao 2016, Shi et al. 2018), cotton-based ACF (Duan et al. 2017), cellulose-based ACF (Simsek et al. 2017, Hina et al. 2018) and so on. However, the prepared ACF is mainly microporous with the narrow pore size distribution (Li and Ma 2013). At the same time, the low specific surface area and single surface structure of ACF also limit its applications in some areas especially those that are requiring adsorption of bulky molecules from solution (Ma and Zhang 2015). In view of the mentioned shortcomings of ACF, it is imminent to prepare the ACF with double surface area structures and increase the adsorption property significantly.

In this paper, the objective of this study was to prepare activated carbon hollow fibers from liquefied rubber wood (WACHF) with double surface area structures. The structures of WACHF were studied by scanning electron microscope (SEM), X-ray diffraction (XRD) and N_2 adsorption. In addition, the adsorption characteristics of the obtained samples were also investigated which methylene blue (MB) and iodine were used as representative adsorbates.

MATERIAL AND METHODS

Rubber wood (*Hevea brasiliensis*) used in this study as a raw material was sourced from Hainan, China. Prior to use, the sample was air dried, grounded in high-speed rotary cutting mill and then screened to give the fraction of $0.2 < Dp < 0.8$ mm particle size for use in the experiments. All other chemicals in the study were reagent grade and they were used without further purification.

The precursor fibers from rubber wood, preparing by previously research (Ma and Zhang 2015), were half-cured by soaking in an acid solution with CH_2O and HCl (1:1 by volume) as main components at 95°C for 5 h. Subsequently, the half-cured fibers were immersed into 18.5% methanol solution at 50°C for 0.5 h, washed with distilled water and dried to obtain the hollow half-cured fibers. Then, wood hollow fiber (WHF) was obtained after the second curing under

the same conditions described in the first step. The as-prepared WHF was activated in a tubular furnace with a temperature program from room temperature to the final activation temperature (500°C, 600°C, 700°C and 800°C, respectively) using a heating rate of 5°C·min^{-1} under N_2 (200 cm^3 min^{-1}), held isothermally for 40 min under a steam flow of 8 g·min^{-1}, and then cooled to room temperature to obtain the WACHF. The WACHF samples were referred as WACHF-500, WACHF-600, WACHF-700, and WACHF-800, respectively.

Surface morphology of the samples was examined by the field emission-scanning electron microscopy (NanoSEM430, FEI, Netherlands). The X-ray diffraction (XRD) patterns of the samples were obtained with a diffractometer (D/max-2500, Japan Rigaku) using Cu Ka radiation (λ=0.154 nm, powdery samples) at 40 kV and 100 mA by step-scanning over the range of 5-60° (*2θ*). The surface area and the porosity of the samples were determined by N_2 adsorption-desorption isotherm measured at 77 K in a Micromeritics ASAP-2020 apparatus.

The Methylene Blue (MB, $C_{20}H_{19}ClN_4$) removal was obtained from an adsorption test where 0.1 g of WACHF was added to a 120 mL flask containing 500 mL of a MB solution with an initial concentration of 300 mg·L^{-1} and shaken at 240 rpm for 1 h at room temperature (25°C). The final MB concentration was determined using a UV-vis spectrophotometer (UV-1600, Meipuda Crop., China) by measuring the light absorbance at a wavelength of 665 nm. The determination of iodine adsorption was carried out following GB/T12496. 8-1999.

RESULTS AND DISCUSSION

Fig. 1 shows the surface and cross-section image of WHF (Fig. 1a-c) and WACHF (Fig. 1d-f). As can be seen from Fig. 1a, WHF has a smooth surface and uniform thickness without surface deposits. After carbonization and activation, the WACHF shows less defects and smoother surface (Fig. 1d), which may be due to the exclusion of non-carbon components forms compact structures and holes inside fibers at high temperature. Fig. 1b and 1e show that both WHF and WACHF have a hollow fibrous structure. After activation, WHF still retains the hollow microstructure. The average hollowness of WACHF is 76.43%. In addition, a lot of irregular deposits are wrapped on the inner surface of WHF (Fig. 1b and c). It may be caused by a series of reactions occur when the fibers impregnate in methanol solution before second curing. After carbonization and activation, these deposits are transformed into regular cylindrical shapes (Fig. 1e and f).

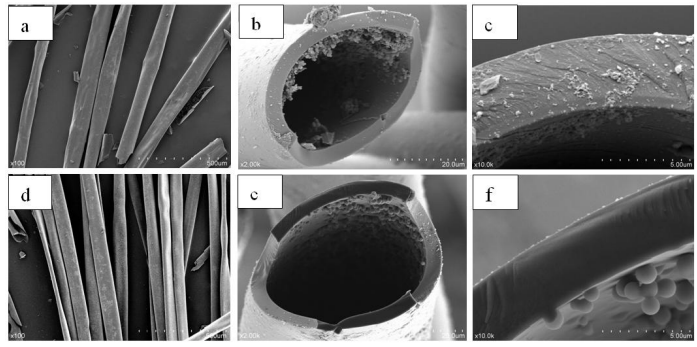

Fig. 1: SEM of WHF (a,b,c) and WACHF (d,e,f).

Fig. 2 shows XRD patterns of WACHF at various activation temperatures. With increased activation temperature, 002 peaks obviously shift from 16.8° at 500°C to 21.7° at 800°C.

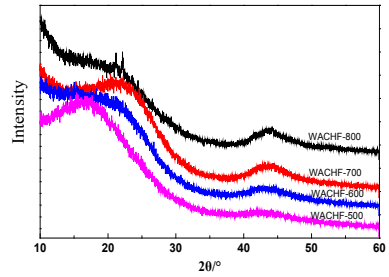

Fig. 2: XRD of WACHF at various temperatures.

When the activation temperature reaches 800°C, the (002) diffraction peaks become narrow and sharp. The 100 peaks of disordered graphite microcrystals at 43.6° also are narrowed and become more prominent as the temperature increasing (Kubo et al. 2007). It indicates that the high activation temperature makes the structure of WACHF tend to be ordered. As shown from the XRD structure parameters (Tab. 1), the values of d_{002}, $L_{c(002)}$ and $L_{a(100)}$ are calculated by using the Scherrer and Bragg formula (Johnson and Frank 1980, Cuesta et al. 1998), respectively d_{002} can be used to evaluate the crystallite degree of carbon materials.

Tab. 1: XRD structure parameters for WACHF at various activation temperatures.

Samples	d_{002}/nm	$L_{c(002)}$/nm	$L_{a(100)}$/nm	$L_{c(002)}/d_{(002)}$
WACHF-500	0.5252	0.8375	3.041	1.595
WACHF-600	0.4421	0.9944	3.124	2.249
WACHF-700	0.4213	0.9140	3.195	2.169
WACHF-800	0.4081	1.036	3.243	2.539

From the calculation results, the increase of the activation temperature from 500 to 800°C leads to an obvious decrease in d_{002} from 0.5252 to 0.4081 nm. It suggests that the crystallite degree is enhanced. In addition, the $L_{c(002)}$, $L_{a(100)}$ and L_c/d_{002} increased from 0.8375 to 1.036 nm, from 3.041 to 3.243 nm and from 1.595 to 2.539 nm, respectively. These results indicate that graphite-like microcrystalite structure and more regular and ordered carbon structure have been formed during the carbonization and activation process. It can be seen that higher activation temperature is conducive to the structure transformation of WACHF from amorphous state to microcrystalline state, and gradually to form graphite like microcrystalline.

Fig. 3 shows the N_2 adsorption-desorption isotherms of WACHF at various activation temperatures. The adsorption isotherm of WACHF is typical type I, based on the IUPAC classification where microporous adsorption is dominating (Ge et al. 2016, Jin et al. 2016, Moreno-Anguiano et al. 2018). The adsorption-desorption curves basically coincide, there is no obvious hysteresis loop, which also indicates that the samples contain a large number of micropores. In addition, when the activation temperature is 800°C, the curve shifts upwards at the maximum pressure, indicating that the samples at this temperature have some mesopores and macropores.

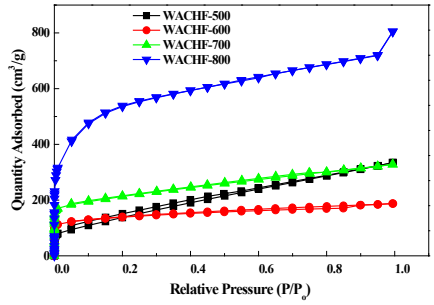

Fig. 3: Nitrogen adsorption-desorption isotherms of WACHF at various temperatures.

The textural parameters of WACHF are listed in Tab. 2. As the activation temperature is increased from 500°C to 800°C, the S_{BET}, S_{micro}, S_{meso}, V_{tot}, V_{micro} and V_{meso} all show increasing trends and have a greater increase at 700 to 800°C. It indicates that with increased activation temperature, carbonization and activation reaction are more intense of WACHF, the exclusion of non-carbon atoms is more complete. And more carbon is eroded to develop the porosity, so the yield of WACHF via activation has an obvious decrease from 57.3 to 22.7%, which almost decreases by 56.9%. The main pore-forming activation temperature for WACHF is 700-800°C.

Tab. 2: The textural parameters of WACHF at various activation temperatures.

Samples	S_{BET} ($m^2\ g^{-1}$)	S_{micro} ($m^2\ g^{-1}$)	S_{meso} ($m^2\ g^{-1}$)	V_{tot} ($cm^3\ g^{-1}$)	V_{micro} ($cm^3\ g^{-1}$)	V_{meso} ($cm^3\ g^{-1}$)	MP-ratio (%)	yield (%)
WACHF-500	409	314	45	0.217	0.157	0.017	72.4	57.3
WACHF-600	510	380	103	0.290	0.161	0.114	55.5	53.0
WACHF-700	764	421	251	0.507	0.273	0.182	53.8	47.7
WACHF-800	1939	1369	436	1.246	0.591	0.577	47.4	22.7

[1] S_{BET}, Brunauer-Emmett-Teller surface area; S_{micro}, micropore surface area; S_{meso}, mesopore surface area; V_{tot}, total pore volume; V_{micro}, micropore volume; V_{meso}, mesopore volume; and MP-ratio = $(V_{micro}/V_{tot}) \times 100\%$.

Fig. 4 shows MB adsorption and iodine adsorption of WACHF at various activation temperatures. With increased activation temperature, MB adsorption and iodine adsorption increase from 5.4 $mg{\cdot}g^{-1}$ and 442.7 $mg{\cdot}g^{-1}$ to 412.6 $mg{\cdot}g^{-1}$ and 1123.7 $mg{\cdot}g^{-1}$, respectively. When the activation temperature is increased from 700 to 800°C, both the MB adsorption and iodine adsorption of WACHF have an obvious increase, which increase by 96.27% and 43.94%, respectively. It indicates that 700°C is the demarcation point of the low temperature carbonization and high temperature carbonization.

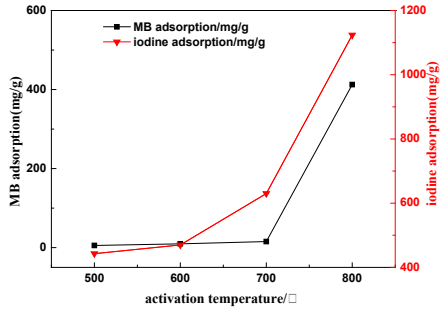

Fig. 4: MB adsorption and iodine adsorption of WACHF at various temperatures.

During high temperature carbonization, the physical structure of WACHF is destroyed, and a more stable graphite structure is formed (Sun et al. 2015). When the temperature reaches 800°C, the water vapor erodes into the interior of WACHF and begins to form a large number of micropores and mesopores, resulting in the adsorption property increasing significantly. The adsorption property of WACHF for iodine is better than MB, it is mainly because the micropores have good adsorption for small molecule iodine and mesopores have good adsorption for macromolecular MB.

CONCLUSIONS

In this study, WACHF samples are successfully synthesized by the phenol liquefaction of rubber wood, melt spinning, curing, methanol solution immersion, as well as second curing and high temperature activation by H_2O. Both WHF and WACHF have a smooth surface and hollow fibrous structure. WACHF has an apparent (002) and (100) diffraction peaks. With increased activation temperature, the value of d_{002} decreases, nevertheless, the $L_{c(002)}$, $L_{a(100)}$ and Lc/d_{002} are increased. WACHF gradually forms graphite-like microcrystalline structure. With increased activation temperature, the S_{BET}, S_{micro}, S_{meso}, V_{tot}, V_{micr}o and V_{meso} all show increasing trends. The prepared material mainly had micropores as well as a few mesopores and macropores. The MB adsorption and iodine adsoption of WACHF also increase. At 800°C, the MB adsorption and iodine adsorption of WACHF reach the maximal values of 412.6 mg·g^{-1} and 1123.7 mg·g^{-1}, respectively.

ACKNOWLEDGMENT

This research has been financially supported by Opening Project Fund of Key Laboratory of Rubber Biology and Genetic Resource Utilization, Ministry of Agriculture / State Key Laboratory Breeding Base of Cultivation & Physiology for Tropical Crops / Danzhou Investigation & Experiment Station of Tropical Crops, Ministry of Agriculture (RRI-KLOF201801), and the National Natural Science Foundation of China (No. 31270607).

REFERENCES

1. Cuesta, A., Dhamelincout, P., Laureyns, J., Martinezalonso, A., Tascon, J.M.D., 1998: Comparative performance of X-ray diffraction and Raman microprobe techniques for the study of carbon materials. Journal of Materials Chemistry 8(8): 2875-2879.

2. Diez, N., Diaz, P., Alvarez, P., Gonzalez, Z., Granda, M., Blanco, C., Santamarıa, R., Menendez, R., 2014: Activated carbon fibers prepared directly from stabilized fibers for use as electrodes in supercapacitors. Material Letter 136: 214-217.
3. Duan, X.H., Srinivasakannan, C., Wang, X., Wang, F., Liu, X.Y., 2017: Synthesis of activated carbon fibers from cotton by microwave induced H_3PO_4 activation. Journal of the Taiwan Institute of Chemical Engineers 70: 374-381.
4. Ge, X.Y., Wu, Z.S., Wu, Z.L., Yan, Y.J., Cravotto, G.C., Ye, B.C., 2016: Microwave-assisted modification of activated carbon with ammonia for efficient pyrene adsorption. Journal of Industrial and Engineering Chemistry 39: 27-36.
5. Hamada, T., Nishida, T., Furuyama, M., Tomioka, T. 1988: Transverse structure of pitch fiber from coal tar mesophase pitch. Carbon 26(6): 837-841.
6. Hina, K.Z., Zou, H.T., Qian ,M W., Zuo, D.Y., Yi, C.H., 2018: Preparation and performance comparison of cellulose-based activated carbon fibres. Cellulose 25(1): 607-617.
7. Jin, G., Eom, Y.J., Lee, T.G., 2016: Removal of Hg(II) from aquatic environments using activated carbon impregnated with humic acid. Journal of Industrial and Engineering Chemistry 42: 46-52.
8. Johnson, D.J., Frank, C., 1980: Recent advances in studies of carbon fiber structure. Philosophical Transactions of the Royal Society 294(1411): 443-449.
9. Kubo, S., Yoshida, T., Kadia, J.F., 2007: Surface porosity of lignin/PP blend carbon fibers. Journal of Wood Chemistry and Technology 27(3-4): 257-271.
10. Kwiatkowski, M., 2017: Analysis of the microporous structure of the low-cost activated carbon fibres obtained from flax and jute cloth. Journal of Mathematical Chemistry 55(10): 1893-1902.
11. Li, C.Y., Wang, W.J., Wang, Y.L., Jiang, X.Q., Han, L.M. 1998: Antibacterial pitch-based activated carbon fiber supporting silver. Carbon 36(1-2): 61-65.
12. Li, D.N., Ma, X.J., 2013: Preparation and characterization of activated carbon fibers from liquefied wood. Cellulose 20(4): 1649-1656.
13. Lin, J., Zhao, G.J., 2016: Preparation and characterization of high surface area activated carbon fibers from lignin. Polymers 8(10): 369.
14. Liu, X.Y., Ma, X.J., Zhu, L.Z., Li, D.N., 2015: Photocatalysis, microstructure, and surface characterization of TiO_2-loaded wooden-activated carbon fibers. Polymer Composites 36(1): 62-68.
15. Ma, X.J., Zhang, F., 2015: Effect of wood charcoal contents on the adsorption property, structure, and morphology of mesoporous activated carbon fibers derived from wood liquefaction process. Journal of Materials Science 50(4): 1908-1914.
16. Moreno-Anguiano, O., Rutiaga-Quinones, J.G., Marquez-Montesino, F., Rico-Cerda, J.L., Carrillo-Parra, A., 2018: Performance of activated carbon obtained from pine wood and determination of its adsorption capacities of ammonia and gasoline vapors. Wood Research 63(6): 1003-1012.
17. Qoi, C.H., Cheah, W.K., Sim, Y.L., Pung, S.Y., Yeoh, F.Y., 2017: Conversion and characterization of activated carbon fiber derived from palm empty fruit bunch waste and its kinetic study on urea adsorption. Journal of Environmental Management 197: 199-205.
18. Rombaldo, C.F.S., Lisboa, A.C.L., Mendez, M.O.A., Coutinho, A.R., 2014: Brazilian natural fiber (jute) as raw material for activated carbon production. Anais Da Academia Brasileira De Ciencias 86(4): 2137-2144.
19. Ryu, Z., Zheng, J.T., Wang, M.Z., 1998: Porous structure of PAN-based activated carbon fibers. Carbon 36(4): 427-432.

20. Shi, X.J., Wang, X., Tang, B., Dai, Z., Chen, K.F., Zhou, J.H., 2018: Impact of lignin extraction methods on microstructure and mechanical properties of lignin- based carbon fibers. Journal of Applied Polymer Science 135(10): 45580-45727.
21. Shrestha, S., Son, G., Lee, S.H., Lee, T.G., 2013: Isotherm and thermodynamic studies of Zn (II) adsorption on lignite and coconut shell- based activated carbon fiber. Chemosphere 92(8): 1053-1061.
22. Shrestha, S., Son, G., Lee, S.H., 2014: Kinetic parameters and mechanism of Zn (II) adsorption on lignite and coconut shell-based activated carbon fiber. Journal of Hazardous, Toxic and Radioactive Waste 18(4): A4014003.
23. Simsek, E.B., Novak, I., Sausa, O., Berek, D., 2017: Microporous carbon fibers prepared from cellulose as efficient sorbents for removal of chlorinated phenols. Research on Chemical Intermediates 43(1): 503-522.
24. Sun, D., Hao, X., Chen, X., Huang, X., 2015: Effects of carbonization temperature on chemical and microcrystalline structural change in wood-ceramics prepared from liquefied pine wood and wood powder. Wood and Fiber Science 47(2): 171-178.
25. Tan, I.A.W., Hameed, B.H., Ahmad, A.L., 2007: Equilibrium and kinetic studies on basic dye oil palm fiber activated carbon. Chemical Engineering Journal 127(1): 111-119.
26. Thitame, P.V., Shukla, S.R., 2016: Adsorptive removal of reactive dyes from aqueous solution using activated carbon synthesized from waste biomass materials. International Journal of Environmental Science and Technology 13(2): 561-570.
27. Yu, B.J., Chang, Z.Z., Wang, C.Y., 2016: The key pre-pyrolysis in lignin- based activated carbon preparation for high performance supercapacitors. Materials Chemistry and Physics 181: 187-193.

Dong-Na Li
Tianjin University of Science and Technology
College of Packaging and Printing Engineering
Tianjin 300222
China

Jia-Ning Li
Chinese Academy of Tropical Agricultural Sciences
Rubber Research Institute
Ministry of Agriculture Key Laboratory of Biology
and Genetic Resource Utilizationof Rubber Tree
State Key Laboratory Breeding Base of Cultivation
and Physiology For Tropical Crops
Danzhou 571737
China

*Xiao-Jun Ma
Tianjin University of Science and Technology
College of Packaging & Printing Engineering
Tianjin 300222
China
*Corresponding author: mxj75@tust.edu.cn